

Conduction Block in One-Dimensional Heart Fibers

Jeffrey J. Fox, Robert F. Gilmour, Jr., and Eberhard Bodenschatz*

Laboratory of Atomic and Solid State Physics and Department of Biomedical Sciences, Cornell University, Ithaca, New York 14853
(Received 10 April 2002; published 16 October 2002)

We present a nonlinear dynamical systems analysis of the transition to conduction block in one-dimensional cardiac fibers. We study a simple model of wave propagation in heart tissue that depends only on the recovery of action potential duration and conduction velocity. If the recovery function has slope ≥ 1 and the velocity recovery function is nonconstant, rapid activation causes dynamical heterogeneity and finally conduction block away from the activation site. This dynamical mechanism may play a role in the initiation and breakup of spiral waves in excitable media.

DOI: 10.1103/PhysRevLett.89.198101

PACS numbers: 87.19.Hh, 05.45.-a, 82.40.Ck

Complex spatiotemporal patterns, including spatiotemporal chaos, are found in a broad class of driven systems [1,2]. A pattern of particular interest is ventricular fibrillation, a heart rhythm disturbance in which disordered wave propagation causes a fatal disruption of the synchronous contraction of the ventricle. Ventricular fibrillation is thought to be a state of spatiotemporal chaos consisting of the perpetual nucleation and disintegration of spiral waves [3,4], in association with a period doubling bifurcation of local electrical properties [5–8]. Nucleation of the initiating spiral wave pair is caused by local conduction block (wave break) secondary to spatial heterogeneity of electrical properties [3,4,9]. Although intrinsic heterogeneity exists in the ventricle [10], purely dynamical heterogeneity is sufficient to cause conduction block in one-dimensional models [11,12]. It has also been shown experimentally that rapid periodic pacing produces dynamic spatiotemporal heterogeneity of cellular electrical properties and conduction block in canine Purkinje fibers [11]. These behaviors result from the interplay between local period-2 dynamics and conduction velocity dispersion. Previous work has thoroughly explored the transition from a homogeneous state in which the period-2 dynamics is manifest as concordant alternans to a spatially heterogeneous state in which the alternans are discordant [12].

In this Letter, we concentrate on the transition from discordant alternans to conduction block. We present a novel nonlinear dynamical systems analysis which shows that discordant alternans and conduction block depend on two dynamical ingredients. One is a monotonically increasing conduction velocity function. The other is a period doubling bifurcation that can arise when a recovery system is driven sufficiently rapidly. We show numerically and analytically that these dynamical ingredients force an initially homogeneous system (concordant alternans) into a spatially heterogeneous state (discordant alternans), and finally to a state in which conduction block occurs away from the activation site.

The recovery properties for action potential duration (D) and conduction velocity (V) are determinants of the dynamics of wave propagation in cardiac tissue (Fig. 1). D

and V for a given action potential (D_{n+1} and V_{n+1} , respectively) are functions of the preceding rest interval (I_n) between action potentials [13–16]. If the recovery function $D_{n+1} = f(I_n)$ has a slope ≥ 1 , a period doubling bifurcation occurs as the time interval between activations is shortened [13–16]. This bifurcation is manifest as a beat-to-beat, long-short alternation of D and I called alternans. Alternation of I also causes an alternation of V , where $V_{n+1} = c(I_n)$ is the conduction velocity recovery function. Alternation of V influences action potential propagation and the spatial distribution of D along a

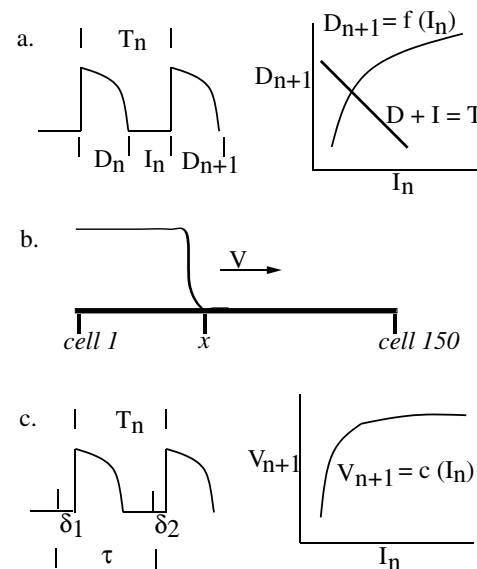


FIG. 1. Schematic diagrams to illustrate the determinants of wave propagation dynamics in cardiac tissue. (a) Left: action potentials in a single cell. Right: action potential duration recovery. The dynamics of a cell are determined by its D recovery function and by the local activation interval T through the relationship $T_n = I_n + D_n$. (b) An activation wave propagates down a 1D fiber made up of 150 coupled cells. (c) Left: the local activation interval at a particular site x is determined by the pacing period τ and by the conduction delays (δ_1 and δ_2) required for a wave to reach that site. Right: conduction velocity recovery. The conduction delays are determined by the conduction velocity recovery function.

cardiac fiber [17,18], such that the long-short D pattern at one end of the fiber reverses phase and becomes a short-long pattern at the other end. This phenomenon, known as discordant alternans, has been observed in experimental studies in isolated hearts [19,20] and heart fibers [11], as well as in simulations of homogeneous one-dimensional cables [17,18] and coupled-map lattices [12,17,18]. If the time interval between activations is decreased further, a transition to local 2:1 conduction block occurs [11,12]. It should be noted that discordant alternans need not necessarily be involved in the transition to 2:1 block, as has been observed in, for example, Ref. [21].

The model we have used to study these dynamical behaviors is a coupled-map model of a one-dimensional cardiac fiber [12,22,23], based on the equation

$$I_{n+1}(x_i) = T_{n+1}(x_i) - D_{n+1}(x_i). \quad (1)$$

$T_{n+1}(x_i)$ is the time interval between activations of site x_i . It is determined by including the time delays caused by the propagation from the pacing site to site x_i . This yields

$$T_{n+1}(x_i) = \tau + \sum_{j=0}^i \frac{\Delta x}{V_{n+1}(x_j)} - \frac{\Delta x}{V_n(x_j)}, \quad (2)$$

where τ is the time interval between activations applied to the pacing site and $\Delta x = 0.1$ is the length of a single cell (time units in msec and space units in mm). The conduction velocity $V_n(x_i)$ depends only on I through the velocity recovery function $V_n = c(I_n)$ given by $c(I) = 0.5(1.430 - 1.150e^{-0.075I} + 0.670e^{-0.150I} - 1.340e^{-0.225I})$. The D recovery function is $f(I) = \frac{220}{1+e^{(20-I)/40}}$ with conduction block modeled by setting $f(I) = 0$ for $I < I_{\min} = 2$. All parameters were taken from Ref. [11] and chosen to produce semiquantitative agreement with experiments done in Purkinje fibers. [The exact form of these equations and choice of parameters are not important. Similar results are obtained from other functions chosen to have different algebraic forms but similar shapes, such as $f(I) = 88 + \frac{122}{1+e^{(40-I)/28}}$ and $c(I) = 0.7(1 - e^{(2-I)/10})$.] Coupling between sites is included using a weighted averaging of $D_{n+1}(x_i)$ [23]: $D_{n+1}(x_i) = \sum_{j=-\alpha}^{\alpha} e^{-\mu j^2} f[I_n(x_{i+j})] / \sum_{j=-\alpha}^{\alpha} e^{-\mu j^2}$ with $\alpha = 50$, $\mu = 0.06$. If the index α falls outside the length of the cable (150 cells), that term is not included in the sums. Weighted averaging models the electrotonic current that flows out of (into) a cell and into (out of) its neighbor if the action potential of the first cell is longer (shorter) than that of its neighbor. The defining equation for the model is therefore

$$I_{n+1}(x_i) = \tau + \sum_{j=0}^i \frac{\Delta x}{c[I_{n+1}(x_j)]} - \frac{\Delta x}{c[I_n(x_j)]} - D_{n+1}(x_i). \quad (3)$$

Numerical iteration of Eq. (3) produced discordant alternans and conduction block similar to experimental observations, as has been reported elsewhere [11].

Analysis of this model is complicated by the spatial averaging term in Eq. (3). If we eliminate spatial averaging from the model for analytic simplicity, we obtain

$$I_{n+1}(x_i) = \tau + \sum_{j=0}^i \frac{\Delta x}{c[I_{n+1}(x_j)]} - \frac{\Delta x}{c[I_n(x_j)]} - f[I_n(x_i)]. \quad (4)$$

Iteration of this difference equation produces discordant alternans [Fig. 2(a)], although, as discussed in [12], the transition between long-short and short-long regions is discontinuous. If we continue to decrease the activation interval, conduction block occurs [Fig. 2(b)]. Thus, the coupling term is not required for conduction block.

We develop an analytical understanding of the mechanism for conduction block by making two simplifying assumptions to Eq. (4). First, we take the continuum limit, turning the sums into integrals. Second, we take a derivative with respect to space, producing an infinite system of coupled ordinary differential equations (ODEs), one ODE for each value of the index n

$$\frac{d}{dx} I_{n+1}(x) = \frac{1}{c[I_{n+1}(x)]} - \frac{1}{c[I_n(x)]} - f'[I_n(x)] \frac{d}{dx} I_n(x), \quad (5)$$

where $f'(I) = \frac{\partial f}{\partial I}$. Next, we seek a period-2 solution in time, which reduces the problem to two coupled ODEs

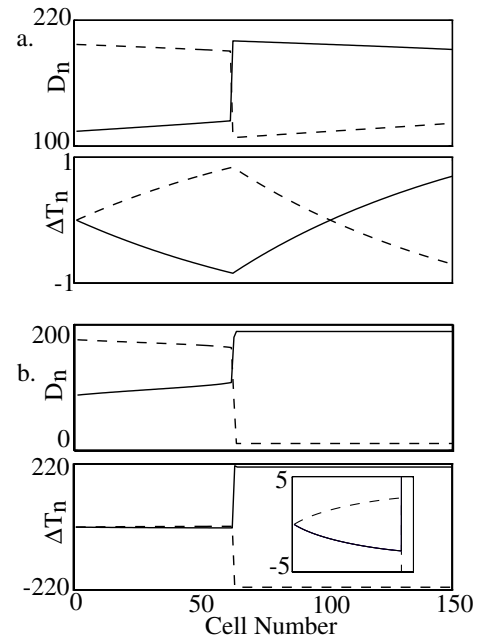


FIG. 2. D_n and $\Delta T_n = T_n - \tau$ versus cell number in the no spatial coupling model for two consecutive beats (dashed line, beat n ; solid line, beat $n+1$). Stimuli were delivered to cell 1 and activation propagated to cell 150. $\tau = 220$ msec in (a), 210 msec in (b). (a) Steady state discordant D alternans. Note the discontinuity in D_n . (b) Steady state 2:1 conduction block. The inset shows the T differences in the first 70 cells.

$$\frac{d}{dx} I_1(x) = \left(\frac{1}{c[I_1(x)]} - \frac{1}{c[I_2(x)]} \right) \frac{\{1 + f'[I_2(x)]\}}{\{1 - f'[I_1(x)]f'[I_2(x)]\}}, \quad (6)$$

$$\frac{d}{dx} I_2(x) = \left(\frac{1}{c[I_2(x)]} - \frac{1}{c[I_1(x)]} \right) \frac{\{1 + f'[I_1(x)]\}}{\{1 - f'[I_1(x)]f'[I_2(x)]\}}. \quad (7)$$

We now treat this as a dynamical system (with x playing the role of time) and analyze the system in the (I_1, I_2) plane. We identify four constraints of motion in the plane. (i) Conduction requires that the intervals I_1 and I_2 are $> I_{\min}$ [Fig. 3(a)]. (ii) Period-2 solutions are unstable if

$$|f'(I_1)f'(I_2)| \geq 1 \quad (8)$$

[Fig. 3(a)]. This condition is obtained from the linear stability of the period-2 solution. (iii) The first cell in the fiber (boundary condition at $x = 0$) has an activation interval T equal to τ . Therefore, at $x = 0$, we have

$$\tau = T_1 = I_1 + D_1 = I_1 + f(I_2), \quad (9)$$

$$\tau = T_2 = I_2 + D_2 = I_2 + f(I_1), \quad (10)$$

$$I_1 + f(I_2) = I_2 + f(I_1). \quad (11)$$

The boundary condition defines a curve in phase space on which the first cell lies [Fig. 3(b)]. Equation (9) describes a two-dimensional surface in (I_1, I_2, τ) space. Equation (10) is a reflection of that surface through the plane $I_1 = I_2$. Thus, the boundary condition Eq. (11) is the

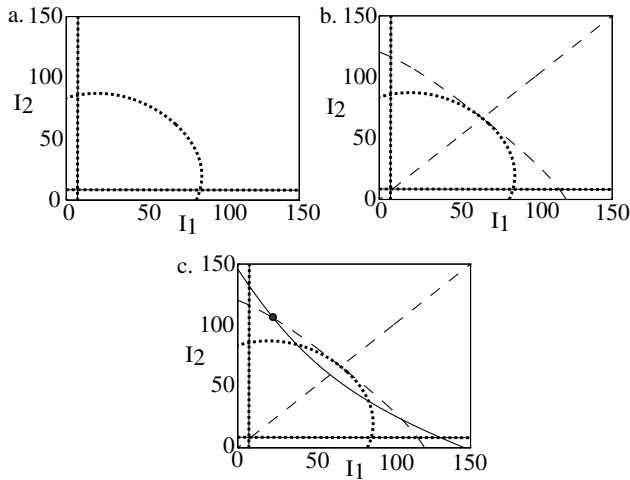


FIG. 3. Phase plane constraints. (a) The short-dashed curve is the stability boundary for period-2 solutions, given by Eq. (8). Inside this curve period-2 solutions are unstable. The vertical and horizontal short-dashed lines are at I_{\min} . These lines and the stability curve also appear in (b) and (c). (b) The long-dashed curves are the boundary conditions for $x = 0$ given by Eq. (11). The long-dashed diagonal is the period-1 solution, while the long-dashed curve is the period-2 solution. These curves also appear in (c). (c) The solid curve is the period-2 curve given by Eq. (12) with $\tau = 220$ msec. The dot is the first cell in the fiber.

intersection of these surfaces projected onto the (I_1, I_2) plane. (iv) To fix the initial condition at $x = 0$, we require that the solution is period 2 in time with a period of 2τ . This gives

$$I_1 + f(I_1) + I_2 + f(I_2) = 2\tau. \quad (12)$$

This equation describes another surface in (I_1, I_2, τ) space. Choosing a specific τ slices this surface, yielding the period-2 curve. Because we look only for period-2 solutions [Eqs. (6) and (7)], every point on the fiber lies on this curve [solid curve in Fig. 3(c)]. The intersection of the period-2 curve with the boundary condition constraint defines the location of the first cell in the fiber. (The intersection with the diagonal is the unstable period-1 solution and is ignored.) These constraints depend only on the D recovery function. The V recovery function plays a role in determining the flow on the period-2 curve. As one moves down the fiber, the flow in phase space is toward the diagonal $I_1 = I_2$ [for example, if $I_1 > I_2$, then this follows from Eqs. (6) and (7) because $c(I)$ is monotonically increasing] [Fig. 4(a)]. The critical length for discordant alternans is thus the distance traveled along the fiber until the period-2 instability is reached [Fig. 4(a)]. Calculating this distance by integrating Eqs. (6) and (7) is difficult, due to singular behavior at the instability boundary. If the length of the cable is shorter than this critical length, then all cells on the fiber lie on the same side of the diagonal, corresponding to concordant alternans. To deduce the trajectory of the system after encountering the

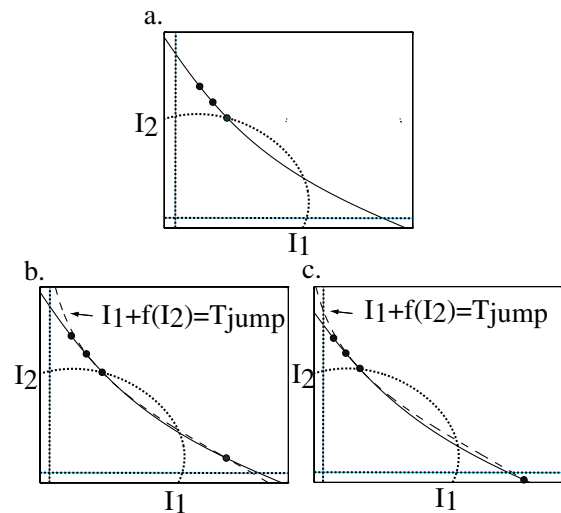


FIG. 4. Mechanism for conduction block. Axes are the same as in Fig. 3. $\tau = 220$ msec in (a) and (b), 210 msec in (c). (a) The solid line is the period-2 curve. The short-dashed curve is the stability boundary, and the vertical and horizontal lines are I_{\min} . These curves also appear in (b) and (c). Flow along the period-2 curve is toward the unstable region. The dots on the period-2 curve correspond to three cells along the fiber in the “concordant” region before the point of discontinuity. The stimulus site is cell 1. (b) Discordant alternans. The long-dashed curve is $T_{\text{jump}} = I_1 + f(I_2)$. (c) Conduction block.

unstable region given by Eq. (8), we note that the local activation interval remains continuous through the discontinuous jump in D (see Fig. 2). We therefore plot the curve $I_1 + f(I_2) = T_{\text{jump}}$, where T_{jump} is defined as the local activation period at the point of discontinuity [Fig. 2(a)]. The next cell on the fiber after the point of discontinuity lies on an intersection of this curve with the period-2 curve. It is important to note that all of the constraint curves Eqs. (8)–(12) are reflection symmetric (i.e., symmetric about the $I_1 = I_2$ diagonal). However, the T_{jump} curve is not. As Fig. 4(b) illustrates, this intersection is on the opposite side of the unstable region, producing larger amplitude alternans. The amplitude of alternans on the opposite side of the discontinuity is larger due to the lack of reflection symmetry of the T_{jump} curve. The latter reflects the lack of symmetry in the recovery function $f(I)$ about the bifurcation point where period-2 solutions appear. If the applied activation interval is slightly smaller, then the period-2 curve and the curve $I_1 + f(I_2) = T_{\text{jump}}$ are shifted closer to the origin, causing the intersection of these curves to fall in the forbidden region [Fig. 4(c)].

The above analysis produces exactly the same results as the simulation of the no spatial coupling model in Fig. 2. The exact shapes of the boundary condition and period-2 curves are unimportant. The only critical ingredients are the period-2 instability, the flow toward the diagonal, and the lack of symmetry in the T_{jump} curve. A 2:1 block can also occur in shorter cables without discordant alternans [12,21]. This transition can occur if τ is chosen small enough that the first cell in the fiber (see Fig. 3) falls into the forbidden region where I_1 or I_2 is $< I_{\text{min}}$.

In summary, we have shown that discordant alternans and conduction block can occur in a simple model that includes only an action potential duration recovery function with slope one or greater and a monotonically increasing conduction velocity recovery function. These phenomena have been studied in coupled-map lattices previously [11,12,17,18]. In particular, Echebarria and Karma analytically explored the transition to discordant alternans and found conduction block in numerical simulations [12]. That study, which also included the effect of electrotonic interactions, derived amplitude equations by linearizing the governing equations and expanding about the unstable period-1 solution. The analysis presented here is thus complementary, in that it is the first fully nonlinear analysis of conduction block in heart fibers.

It has been argued that discordant alternans and conduction block require significant intrinsic spatial heterogeneity of cellular electrical properties [19,20]. While

intrinsic spatial heterogeneity is not necessary for conduction block, intrinsic heterogeneity may break the symmetry of wave propagation so that not every point along the wave front blocks at the same time [1,9,20]. Thus, the mechanism for conduction block presented in this Letter may be a mechanism for wave break and the initiation and subsequent breakup of spiral waves in excitable media such as the heart.

These studies were supported by NIH Grant No. HL62543 (R. F. G.) and by an IGERT training grant from the NSF (J. J. F.).

*Electronic address: eb22@cornell.edu

<http://milou.msc.cornell.edu/>

- [1] M. C. Cross and P. C. Hohenberg, *Rev. Mod. Phys.* **65**, 851 (1993).
- [2] J. P. Gollub and M. C. Cross, *Nature (London)* **404**, 710 (2000).
- [3] P. S. Chen *et al.*, *Circ. Res.* **62**, 1191 (1988).
- [4] F. X. Witkowski *et al.*, *Nature (London)* **392**, 78 (1998).
- [5] A. Karma, *Chaos* **4**, 461 (1994).
- [6] R. F. Gilmour and D. R. Chialvo, *J. Cardiovasc. Electrophysiol.* **10**, 1087 (1999).
- [7] A. Garfinkel *et al.*, *Proc. Natl. Acad. Sci. U.S.A.* **97**, 6061 (2000).
- [8] A. Panfilov, *Chaos* **8**, 57 (1998).
- [9] H. Arce *et al.*, *Chaos* **10**, 411 (2000).
- [10] G. X. Yan, W. Shimizu, and C. Antzelevitch, *Circulation* **98**, 1921 (1998).
- [11] J. J. Fox *et al.*, *Circ. Res.* **90**, 289 (2002).
- [12] B. Echebarria and A. Karma, *Phys. Rev. Lett.* **88**, 208101 (2002).
- [13] J. B. Nolasco and R. W. Dahlen, *J. Appl. Physiol.* **25**, 191 (1968).
- [14] M. R. Guevara *et al.*, *IEEE Comp. Cardiol.* **562**, 167 (1984).
- [15] D. R. Chialvo and J. Jalife, *Nature (London)* **330**, 749 (1987).
- [16] D. R. Chialvo, R. F. Gilmour, and J. Jalife, *Nature (London)* **343**, 653 (1990).
- [17] Z. Qu *et al.*, *Circulation* **102**, 1664 (2000).
- [18] M. A. Watanabe *et al.*, *J. Cardiovasc. Electrophysiol.* **12**, 196 (2001).
- [19] J. M. Pastore *et al.*, *Circulation* **99**, 1385 (1999).
- [20] J. M. Pastore and D. S. Rosenbaum, *Circ. Res.* **87**, 1157 (2000).
- [21] T. J. Lewis and M. R. Guevara, *J. Theor. Biol.* **146**, 407 (1990).
- [22] M. Courtemanche, L. Glass, and J. P. Keener, *Phys. Rev. Lett.* **70**, 2182 (1993).
- [23] A. Vinet, *Ann. Biomed. Eng.* **28**, 704 (2000).